Original Article

Sargassum polysaccharide attenuates osteoarthritis in rats and is associated with the up-regulation of the ITGβ1-PI3K-AKT signaling pathway

Yanzhi Liu [**,1], Rui Lin [1], Haiping Fang [1], Lixian Li, Min Zhang, Lujiao Lu, Xiang Gao, Jintong Song, Jinsong Wei, Qixian Xiao, Fucheng Zhang, Kefeng Wu [***], Liao Cui [*]

Zhanjiang Key Laboratory of Orthopaedic Technology and Trauma Treatment, Key Laboratory of Traditional Chinese Medicine for the Prevention and Treatment of Infectious Diseases, Guangdong Key Laboratory for Research and Development of Natural Drugs, School of Pharmacy, School of Ocean and Tropical Medicine, The Affiliated Hospital, The Second Affiliated Hospital, Zhanjiang Central Hospital, Guangdong Medical University, Zhanjiang, China

ARTICLE INFO

ABSTRACT

Background: Osteoarthritis (OA) presents a formidable challenge, characterized by as-yet-unclear mechanical intricacies within cartilage and the dysregulation of bone homeostasis. Our preliminary data revealed the encouraging potential of a Sargassum polysaccharide (SP), in promoting chondrogenesis. The aim of our study is to comprehensively assess the therapeutic effects of SP on OA models and further elucidate its potential mechanism.

Methods: The protective effects of SP were initially evaluated in an inflammation-induced human chondrocyte (C28) cell model. CCK-8 assays, Alcian blue staining, RT-qPCR and Western blotting were used to verify the chondrogenesis of SP *in vitro*. To assess the efficacy of SP *in vivo*, surgically induced medial meniscus destabilization (DMM) OA rats underwent an 8-week SP treatment. The therapeutic effects of SP in OA rats were comprehensively evaluated using X-ray imaging, micro-computed tomography (μ-CT), histopathological analysis, as well as immunohistochemical and immunofluorescent staining. Following these assessments, we delved into the potential signaling pathways of SP in inflammatory chondrocytes utilizing RNA-seq analysis. Validation of these findings was conducted through RT-qPCR and western blotting techniques.

Results: SP significantly enhance the viability of C28 chondrocytes, and increased the secretion of acidic glycoproteins. Moreover, SP stimulated the expression of chondrogenic genes (*Aggrecan*, *Sox9*, *Col2a1*) and facilitated the synthesis of Collagen II protein in C28 inflammatory chondrocytes. *In vivo* experiments revealed that SP markedly ameliorated knee joint stenosis, alleviated bone and cartilage injuries, and reduced the histopathological scores in the OA rats. μ-CT analysis confirmed that SP lessened bone impairments in the medial femoral condyle and the subchondral bone of the tibial plateau, significantly improving the microarchitectural parameters of the subchondral bone. Histopathological analyses indicated that SP notably enhanced cartilage quality on the surface of the tibial plateau, leading to increased cartilage thickness and area. Immunohistochemistry staining and immunofluorescence staining corroborated these findings by showing a significant promotion of Collagen II expression in OA joints treated with SP. RNA-seq analysis suggest that SP's effects were mediated through the regulation of the ITGβ1-PI3K-AKT signaling axis, thereby stimulating chondrogenesis. Verification through RT-qPCR and Western blot analyses confirmed that SP significantly upregulated the expression of ITGβ1, p110δ, AKT1, ACAN, and Col2a1. Notably, knock-down of ITGβ1 using siRNA in C28 chondrocytes inhibited the expression of ITGβ1, p110δ, AKT1, and ACAN. However, these inhibitory effects were not completely reversed by supplemental SP intervention.

---

  * Corresponding author. Guangdong Provincial Key Laboratory for Research and Development of Natural Drug, School of Pharmacy, Guangdong Medical University, Zhanjiang, 524023, China.
  ** Corresponding author. Zhanjiang Key Laboratory of Orthopaedic Technology and Trauma Treatment, Zhanjiang Central Hospital, Guangdong Medical University, Zhanjiang, 524045, China.
  *** Corresponding author. School of Ocean and Tropical Medicine, Guangdong Medical University, Zhanjiang, 524023, China
    E-mail addresses: liuyanzhi02@163.com (Y. Liu), 49095832@qq.com (K. Wu), cuiliao@163.com (L. Cui).
  [1] Yanzhi Liu, Rui Lin and Haiping Fang contributed equally to this work and share first authorship

Conclusions: In summary, our findings reveal that SP significantly enhances chondrogenesis both *in vitro* and *in vivo*, alleviating OA progression both in bone and cartilage. The observed beneficial effects are intricately linked to the activation of the ITGβ1-PI3K-AKT signaling axis.

The translational potential of this article: Our research marks the first instance unveiling the advantageous effects and underlying mechanisms of SP in OA treatment. With its clinical prospects, SP presents compelling new evidence for the advancement of a next-generation polysaccharide drug for OA therapy.

1. Introduction

Osteoarthritis (OA) is a multifaceted and degradative joint disease influenced by various factors [1], impacting the structure of articular cartilage, subchondral bone, ligaments, joint capsule, synovium, and surrounding muscles [2]. It affects over 240 million people globally [3], with the knee being the most frequently affected joint, followed by the hand and hip [2,4]. As of 2020, knee OA has a reported global prevalence of 16.0 % (95 % CI, 14.3%–17.8 %) and an incidence of 203 per 10, 000 person-years (95 % CI, 106–331) [5]. Various factors, including age [6], genetic predisposition [7], obesity [8], gender [9], previous injury [10], sports [11], ethnicity [12] and joint shape [13] are recognized as risk factors for OA. Due to its high prevalence and diverse risk factors, OA is a leading global cause of disability [14]. Cartilage tissue damage, serving as the main indicator for assessing OA progression [1]. Cartilage nearly has no self-repair ability, attributed to the absence of blood vessels and nerve tissue, hinders effective regeneration [15].

Currently, the majority of pharmacological agents primarily offer pain relief and anti-inflammatory effects. Oral non-steroidal anti-inflammatory drugs (NSAIDs), a classic treatment [16], are limited by gastrointestinal [17], cardiovascular [18] and renal toxic effects [19]. Intra-articular therapies, including glucocorticoids [20] and hyaluronic acid (HA) [21] are commonly used but mainly address pain relief and joint lubrication. The challenge persists in effectively treating OA for cartilage repair.

In light of the constraints associated with traditional pharmaceutical preparations, researchers are delving into novel therapeutic agents, including natural bioactive ingredients, to impede the progression of OA [22,23]. The identification of natural bioactive components that promote cartilage regeneration is crucial in preventing the progression of OA [24]. Polysaccharides, serving as natural polymers mirroring the characteristics of the cartilage extracellular matrix (ECM), have attracted attention for the development of OA treatment drugs [25]. While glucosamine has long been used as a supplementary treatment for OA, its efficacy in cartilage formation is considered limited [26,27]. Building on the use of glucosamine in OA treatment, the development of polysaccharide-based drugs with enhanced chondrogenic activity represents a promising strategy.

Sargassum, a versatile genus of brown seaweeds [28], contains polysaccharides with diverse benefits, including anti-inflammatory [29], anti-tumor [30], antioxidant [31], hypoglycemic [32] and hypolipidemic [33]. In a prior study, we highlighted the efficacy of a crude polysaccharide extract from Sargassum in promoting bone formation [34]. Subsequently, a purer Sargassum polysaccharide (SP) was isolated, displaying anti-osteoporosis activity. Its structure was characterized as a polysaccharide consisting mainly of glucose [35]. Based on the structural features of SP similar to glucosamine, we performed some preliminary experiments to evaluate the chondrogenesis effects of SP. The preliminary results suggest SP may have therapeutic potential for OA. Therefore, this study aims to investigate the specific protective effects and potential mechanisms of SP on cartilage repair and OA treatment. Our research identifies SP as a potential anti-OA agent with promising chondrogenic activity.

2. Materials and methods

2.1. Materials and reagents

Thirty 8-week-old, specific-pathogen-free male Sprague–Dawley (SD) rats, weighing 250.00 ± 10.00 g (permit No: SCXK (Beijing)2019-0010) (Purchased from Sibei Fu (Beijing) Biotechnology Co., Ltd., Beijing, China) were fed with standard diet and free access to water with a 12 h light–dark cycle at 25 °C ± 1 °C. The selection of male Sprague–Dawley (SD) rats was based on the widespread practice in osteoarthritis research and the absence of evidence indicating gender-related effects on study outcomes.

The experimental procedures strictly adhered to the guidelines outlined in the "Guide for the Care and Use of Laboratory Animals" by both the Guangdong Laboratory Animal Monitoring Institute and the National Laboratory Animal Monitoring Institute of China. The experimental procedures were conducted in accordance with approved protocols by the Specific Pathogen-Free animal care unit of the Animal Center at Guangdong Medical University, holding the Laboratory Animal Use Permit Number SYXK(粤)2019-0213. Additionally, these procedures were approved by the Academic Committee on the Ethics of Animal Experiments at Guangdong Medical University, Zhanjiang, P.R. China, under Permit Number: GDY2002272.

The C28 chondrocytes line was purchased from Beijing Spectrometric Detection Technology Co., Ltd. Sargassum fusiforme (identified by Dr. Zhanping Gou, Department of Pharmacognosy, Guangdong Medical University, China) was collected from the local wholesale market in Zhanjiang, Guangdong, China. Sargassum polysaccharide (SP), referred to as SFP-1 in the previous research [35], was derived from the extraction and subsequent purification of Sargassum fusiforme. The SP was composed of α-D-Glcp-1→, →4,6)-α-D-Glcp-(1→, and →4)-α-D-Glcp-(1 → . The primary constituent of SP is glucose and its average molecular weight (Mw) is 27,476. The structural formula of SP depicted in Fig. 1, the characterization of SP were shown in our previous study [35]. SP is provided by Marine Medical Research Institute of Zhanjiang.

2.2. Cell culture

C28 cells were seeded into 100 mm cell culture dishes with DMEM high-glucose complete medium and incubated under conditions of 5 % CO_2 concentration, 95 % humidity, and a temperature of 37 °C. During
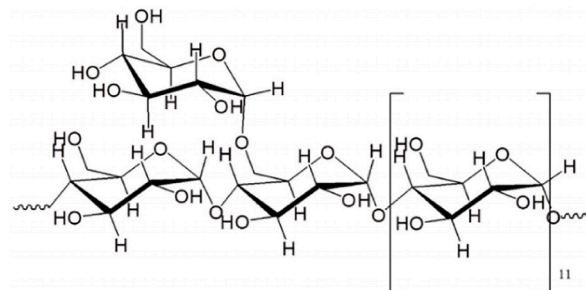

Figure 1. Structural formula of Sargassum polysaccharide (SP) and its average molecular weight (Mw) is 27,476 [35].

the procedures of TNFα modeling and SP administration, the DMEM high-glucose complete medium was utilized as the solvent as well.

2.3. Cell viability assay

C28 chondrocytes were incubated without or with various concentrations of SP in 96-well plates for 24, 48, and 72 h. The culture medium was replaced with fresh medium every two days, and cell viability was quantified using Cell Counting Kit-8 assay (C0038, Beyotime, Shanghai, China).

2.4. TNFα induction

C28 chondrocytes were treated with 1 ng/ml TNFα (10602-HNAE, Beijing Yiqiao Shenzhou Technology Co., Ltd., China), which is known to induce inflammatory injury in chondrocytes. The aim was to simulate the conditions of inflammation in order to assess the therapeutic benefits of SP. The *in vitro* experiment group setting comprised healthy control cells (CON; incubated in complete medium), cells incubated in complete medium containing 1 ng/ml TNFα (TNFα), cells incubated in complete medium containing 1 ng/ml TNFα and 3.2×10^{-4} mg/ml SP (SP).

2.5. Alcian Blue staining

Alcian Blue is a cationic dye that easily binds to anionic groups of cartilage matrix, especially binds to the acidic mucopolysaccharides components of the cartilage matrix. During the staining procedure, the intensity of the Alcian Blue dye's color is directly proportional to the concentration and distribution of acidic mucopolysaccharides in the tissue. Alcian Blue staining is widely accepted as a method for identifying cartilage [36] or for assessing the chondrogenic differentiation potential of cells [37]. C28 chondrocytes were seeded in 12-well plates and cultivated for ten days, with the culture medium was replaced every two days. Following the incubation period, acid mucopolysaccharide content was analyzed using Alcian Blue 8GX staining (A8140, Solarbio, Beijing, China).

2.6. Small interfering RNA transfection

Cells were transfected using Lipofectamine™ 3000 (L3000015, Invitrogen) according to the instruction from the manufacturer. The cells were incubated with small interfering RNAs (siRNA) for 6 h. ITGβ1 siRNA (Gene Pharma, Shanghai, China) was employed for the knockdown of ITGβ1, while RNA interference negative control duplexes (Gene Pharma, Shanghai, China) served as the control siRNA.Post-transfection, the C28 chondrocytes were treated with SP for either 24 or 48 h. Subsequently, RNA and protein were extracted from the cells for analysis by RT-qPCR and Western blot respectively. The sequences for ITGβ1 siRNA were as follows: sense, 5′- GAACAGAUCUGAUGAAUGATT -3′; antisense, 5′- UCAUUCAUCAGAUCUGUUCTT -3′.

2.7. Quantitative reverse transcription-PCR

Total RNA from C28 chondrocytes was extracted using the TRIzol (Takara Bio Inc.). The total RNA served as a template for synthesizing complementary DNA using reverse transcriptase kits (RR036A, Takara Bio Inc., Kusatsu, Japan), in accordance with the manufacturer's guidelines. The relative gene expression levels of *Aggrecan* (*ACAN*), *Sox9*, collagen type II alpha 1 (*Col2a1*), *IL-1β*, *MMP13*, collagen type X alpha 1 (*Col10a1*), β1 integrins (*ITGβ1*), *p110δ*, and *AKT1* were determined using SYBR Green real-time PCR kits (SYBR® Premix Ex Taq™ II, RR820A; Takara Bio Inc.) on an ABI 7500 Fast Real-Time PCR system (Applied Biosystems Life Technologies, Foster City, CA, USA). GAPDH served as the normalization reference. Relative gene expression was quantified using the comparative threshold cycle ($2^{-\Delta\Delta Ct}$) calculation. The PCR reaction conditions were set as: 95 °C for 30 s, followed by 40 cycles of 95 °C for 5 s, and 60 °C for 34 s. Supplementary Table S1 shows the synthesized real-time PCR gene primers.

2.8. Western blotting

Cell lysates were prepared by homogenizing the samples in radio-immunoprecipitation assay (RIPA) buffer (P0013C, Beyotime, Shanghai, China) on ice. Centrifugation at $10,000 \times g$ for 10 min at 4 °C was used to collect the protein samples. Proteins (30 mg/sample) were prepared for SDS-PAGE. The separated proteins were subsequently transferred onto polyvinylidene fluoride (PVDF) membranes (FFP77, Beyotime, Shanghai, China). The membranes were incubated with primary antibodies at 4 °C overnight. The antibodies used included Collagen II (ab188570, Abcam), Aggrecan(ab3778, Abcam), ITGβ1(ab179471, Abcam), PI3Kinase p110δ(ab109006, Abcam), Phospho-AKT1(9018, Cell Signaling Technology), and AKT1(2938, Cell Signaling Technology), all at a 1:1000 dilution. GAPDH (ab181602, Abcam) was utilized as the control at a 1:10,000 dilution. For secondary detection, membranes were incubated with goat anti-rabbit IgG (A21020, Abbkine, at a 1:5000 concentration) for 1 h at 37 °C.The immunoreactive bands were visualized using a FluorChem® Q Imaging System (ProteinSimple, Santa Clara, CA, USA) and the protein expression was quantified by Image J software and normalized to GAPDH.

2.9. RNA sequencing (RNA-seq)

Total RNA from C28 chondrocytes was isolated using the TRIzol assay (Takara Bio Inc.). An aliquot of the RNA samples was denatured at an appropriate temperature to relax their secondary structures, after which mRNA was purified using oligo(dT)-attached magnetic beads. The reaction mixture was then assembled. The RNAs were incubated at the optimal temperature for a set duration, resulting in their fragmentation. Subsequently, the first-strand cDNA synthesis reaction mix was prepared, and the corresponding program was established to synthesize the first-strand cDNA. This step was followed by setting up the second-strand cDNA synthesis reaction system and programming the synthesis of the double-stranded cDNA. Once the reaction mixtures and procedures were in place, the double-stranded cDNA fragments underwent end repair, and an additional 'A' nucleotide was appended to the 3′ ends of the blunt fragments. The adaptor ligation reaction system was then prepared with its specific program to attach adaptors to the cDNA fragments. The PCR amplification was set up next, creating the conditions to amplify the ligated products. The PCR products were denatured to yield single-stranded molecules, which were then circularized through a designated reaction system and procedure. The circularized single-strands that successfully formed were kept, while any uncyclized linear DNA molecules were digested. The single-stranded circular DNA underwent rolling circle amplification to create DNA nanoballs (DNBs), each containing multiple copies of the DNA sequence. These high-quality DNBs were then loaded onto patterned nanoarrays using the high-intensity DNA nanochip technique. Sequencing was carried out using the combinatorial Probe-Anchor Synthesis (cPAS) method on the DNBSEQ platform (BGI). The resulting data were processed and analyzed on the Dr. Tom II network platform provided by BGI (https://biosys.bgi.com/).

2.10. Establishment of OA model

Thirty male SD rats were randomly divided into the following three groups (10 rats/group) according to the body weight range: Sham group (Expose right knee joint without surgery), OA group (The right knee joint was surgically exposed and the DMM was performed to induce OA in rats.) and TNFα + SP group (Treatment of OA rats by intragastric administration of SP).

The SD rat underwent anesthesia via intraperitoneal injection of 2 % sodium pentobarbital at a dosage of 0.13 ml/100 g. The protocol

outlines a comprehensive surgical procedure to induce destabilization of the medial meniscus in SD rats, with the specific steps image in Supplementary Fig. S1: (A) The medial meniscus was rendered accessible by surgically exposing the right knee joint of a SD rat. (B) This exposure allowed for clear visualization of the collateral ligament in the right knee joint. (C) Then an incision was made with ophthalmic scissors to cut through the collateral ligaments, effectively compromising their structural support. (D) A meticulous inspection ensured the ligaments were completely transected. (E) The scissors were carefully positioned between the medial meniscus and the neighboring medial femoral condyle to loosen the medial meniscus. (F) Then the instrument was skillfully guided between the medial meniscus and the tibial plateau to further detach the meniscal tissue. After these procedures, the stability of the medial meniscus is tested using the ophthalmic scissors. A noticeable looseness confirms the successful induction of an unstable state. If the medial meniscus remains stable, steps (E) and (F) must be repeated until the appropriate degree of instability is achieved. Following the surgery, the incision is carefully closed with sutures, and an intraperitoneal injection of sodium penicillin is administered to the rats to reduce the risk of infection, thereby finalizing the surgical model.

Following the DMM procedure, the rats in each groups received daily oral gavage treatments. Previous research has demonstrated that the daily clinical dosage range of glucosamine for humans falls between 1.5 and 3 g [38,39]. When adjusted for rats, this translates to an equivalent dosage range of 140.25–280.5 mg/kg/day. Consequently, in our preliminary experiment (Supplementary Fig. S2), we chose a dosage of 200 mg/kg/day for glucosamine hydrochloride (GH), and administered the same dosage of SP to rats via gavage for 8 weeks. The results from the preliminary experiment indicate that SP has a superior therapeutic effect compared to GH. therefore, we have selected a dosage of 200 mg/kg/day for SP to proceed with the formal experiments in this study.

The Sham and OA groups were administered normal saline via gavage, while the rats in TNFα + SP group received SP at a concentration of 200mg/5 ml/kg through the same method. Eight weeks after initiating treatment, humanely euthanizing the rats through cardiac puncture while under anesthesia.

2.11. Pathological evaluation

Hind limb specimens from the rats were harvested and prepared by meticulously removing any remaining muscles surrounding the femur and tibia. The patella was then excised while carefully preserving the joint capsule. Images of the rat's knee joint were captured using a stereomicroscope for detailed examination. To quantify the extent of osteoarthritic damage, the histopathological scoring standard specific to assessing lesion areas in rat osteoarthritis was employed [40].

2.12. X-ray assessment

The upper portion of the femur and the lower section of the tibia in the rat knee joint were carefully sectioned using a slow saw, ensuring a remaining knee joint length of approximately 2 cm. This preserved segment of the rat's knee joint was then positioned within an X-ray scanner for imaging. X-ray scanning parameters: 40kv, 3.40s, 0.20 mA.

2.13. μ-CT assessment

The rat knee joints were scanned and analyzed using a μ-CT (Viva CT 80, Scanco Medical, Bruettisellen, Switzerland). μ-CT scanning parameters: high resolution (image matrix: 2048 × 2048, integration time: 200 ms, Energy/intensity: 70kVP, 114 μA, 8 W, Voxelsize: 15.6 μm, 1200mgHA/cm). Post-scanning, the positioning of the rat knee joints was adjusted using DataViewer software. The Region of Interest (ROI) was delineated, and the images of bone tissue were quantitatively analyzed using CTAn and Image Pro Plus software. In the μ-CT images, the areas of femoral and tibial plateau injuries appear distinctly dark black, in contrast to the non-injured regions, which are predominantly white. This contrast between the two colors is stark and clear. Consequently, we utilize Image Pro Plus to assess the integrated optical density (IOD) of the damaged area (the black region). The software calculated various parameters including: IOD value of femur damage, IOD value of tibial plateau damage, thickness of subchondral bone plate (SBP.Th, 1/mm), trabecular pattern factor (Tb.Pf, 1/mm), bone volume (BV, mm^3), tissue volume (TV, mm^3), bone volume/tissue volume (BV/TV, %), trabecular number (Tb.N, 1/mm), trabecular thickness (Tb.Th, mm) and trabecular separation (Tb.Sp, mm). Finally, the three-dimensional structure of the bone tissue was generated for visualization using CTvox software.

2.14. Histopathological analysis

Following the completion of the μ-CT scan, the rat knee joints were immersed in a 12 % EDTA solution for decalcification at room temperature for a duration of six weeks. The completion of decalcification was confirmed when a needle could be inserted into the bone tissue without resistance. Subsequent to decalcification, the knee joints underwent a series of dehydration and clarification steps. The process involved a graded series of ethanol treatments beginning with 70 % ethanol for 24 h, followed by 80 % ethanol for 12 h, 90 % ethanol for 2 h, and two consecutive 1-h immersions in 100 % ethanol. Next, the samples were cleared in xylene for 40 min. The dehydration and clearing process was followed by a 2-h soak in soft wax and another 2-h soak in hard wax before being embedded in paraffin. The Rat knee joint sample were embedded in paraffin, sectioned, and stained with Hematoxylin-Eosin (HE) Stain Kit (G1120, Solarbio, China), Toluidine blue (89640, sigma, American) and Saffron-O and Fast Green Stain Kit (G1371, Solarbio, China) at the endpoint for histology analysis.

2.15. Immunohistochemistry

Sections underwent antigen retrieval using a Quick antigen repair solution for frozen sections (P0090, Beyotime, Shanghai, China), followed by the application of an endogenous peroxidase blocking agent (PV-9000, Beijing Zhongshan Jinqiao Biotechnology Co., Ltd., Beijing, China) to quench endogenous peroxidase activity. Post-antigen retrieval, the sections were blocked in a 5 % bovine serum albumin (BSA) (A8010, Solarbio, Beijing, China) solution with 0.3 % Triton X-100 (BS084, Biosharp, China) to prevent nonspecific binding. This was followed by an overnight incubation at 4 °C with a primary antibody, Collagen II Antibody (NB600-844, NOVUS, American). After primary antibody incubation, the sections were treated with a reaction enhancing solution (PV-9000, Beijing Zhongshan Jinqiao Biotechnology Co., Ltd., Beijing, China) and subsequently incubated with a goat anti-mouse/rabbit IgG polymer conjugated to an enhanced enzyme (PV-9000, Beijing Zhongshan Jinqiao Biotechnology Co., Ltd., Beijing, China) for secondary antibody binding. The binding of the antibody was visualized using a DAB chromogenic kit (DA1010, Solarbio, Beijing, China). For the finishing touch, all immunohistochemically stained sections were counterstained with Mayer's Hematoxylin Stain Solution (G1080, Solarbio, Beijing, China). The Integrated Optical Density (IOD) value of the staining was quantified using Image Pro Plus software for analysis.

2.16. Immunofluorescence

Antigen retrieval was performed using a Quick antigen repair solution designed for frozen sections (P0090, Beyotime, Shanghai, China). Following the retrieval process, the sections were blocked in a solution comprising 5 % bovine serum albumin (BSA) (A8010, Solarbio, Beijing, China) with 0.3 % Triton X-100 (BS084, Biosharp, China) to minimize nonspecific antibody binding. This was followed by an overnight incubation at 4 °C with a Collagen II primary antibody (NB600-844, NOVUS,

American). Subsequently, the sections were incubated with Anti-mouse IgG (H + L), F(ab')2 Fragment (Cell Signaling, 4409, American) for 1 h as a secondary antibody to detect the primary antibody binding. After thorough washing, the sections were rapidly dehydrated using 100 % ethanol, dried, and then mounted with an anti-fade mounting medium (Yeasen Biotech, 36308ES20) that contained DAPI to counterstain the nuclei. The prepared sections were then examined and imaged promptly using an ultra-high-resolution confocal microscope (SpinSR10, OLYMPUS), ideally within 1 h at room temperature or up to 4 h when stored at 4 °C to prevent photobleaching. Quantitative analysis of the staining was facilitated by Image Pro Plus software, which computed the Integrated Optical Density (IOD) value of the labeled antigen.

2.17. Statistical analysis

Statistical software SPSS19.0 was used to analyze the data, and independent sample T test and one-way ANOVA were used to analyze the statistical difference. $P < 0.05$ indicates that the difference is statistically significant. GraphPad Prism 8.0 software was used for drawing and analysis.

3. Results

3.1. TNFα induced inflammatory injury to C28 chondrocytes and notable bone and cartilage damage occurred in OA rats

Following TNFα induction, C28 chondrocytes were utilized to establish an inflammatory injury model for chondrocytes. Compared with CON group, the secretion level of acidic glycoprotein in C28 chondrocytes significantly decreased after inflammatory injury ($P < 0.001$) (Fig. 2B). RT-qPCR results indicated that TNFα decreased the gene expression of *Col2a1* and enhanced the gene expression of *IL-1β*, *MMP13* and *Col10a1* in comparison to the CON group (Fig. 3A). Western blot results showed that the expression level of collagen II in TNFα group decreased compared with CON group (Fig. 3B). The model of OA rats induced by DMM surgery. Notably, compared to the Sham group, OA

rats exhibited significant bone and cartilage degradation at the femoral condyle of the medial knee joint, a narrowed knee joint space, and a pronounced increase in the histopathological score for osteoarthritic lesions ($P < 0.001$) (Fig. 4). μ-CT analyses further underscored the injury to the subchondral bone in OA rats, particularly within the medial femoral condyle and the subchondral bone's C region on the tibial plateau, This was evidenced by a considerably reduced trabecular bone volume to tissue volume (BV/TV) ratio, along with substantial impairment of bone geometry and microstructural parameters, including the thickness of the subchondral bone plate, trabecular pattern factor, trabecular number, thickness, and separation, compared to the Sham group (Fig. 5). Moreover, there was a 378.95 % increase in the cartilage degeneration score ($P < 0.01$), alongside a 38.95 % decrease in cartilage thickness ($P < 0.05$) and a 53.59 % reduction in cartilage area ($P < 0.01$), indicating significant damage to the knee cartilage in OA rats (Fig. 6). In addition, the results of immunohistochemistry and immunofluorescence showed that the expression of Collagen II in knee cartilage of OA rats decreased by 79.86 % ($P < 0.001$) and 72.66 % ($P < 0.001$) compared to the Sham group, respectively (Fig. 6).

3.2. SP facilitated the repair of cartilage in C28 inflammatory chondrocytes and ameliorated bone and cartilage injuries in OA rats

Treatment with SP facilitated cartilage repair and ameliorated inflammatory injury in C28 inflamed chondrocytes. The CCK-8 assay demonstrated that SP significantly enhanced the viability of C28 chondrocytes (Fig. 2A). Based on the CCK-8 assay results presented in Fig. 2A, we determined that the optimal concentration of SP for subsequent *in vitro* experiments is 3.2×10^{-4} mg/ml. Compared with TNFα group, the secretion level of acidic glycoprotein in C28 inflammatory chondrocytes increased by 42.75 % after SP intervention ($P < 0.001$) (Fig. 2B). In addition, compared with TNFα group, SP considerably upregulated the gene expression of *Aggrecan*, *Sox9* and *Col2a1* (Fig. 3A) and increased Collagen II protein expression by 54.74 % ($P < 0.05$) (Fig. 3B). The treatment of SP promoted cartilage repair and improved the bone and cartilage injury of OA rats. The femoral condyle of the medial knee joint
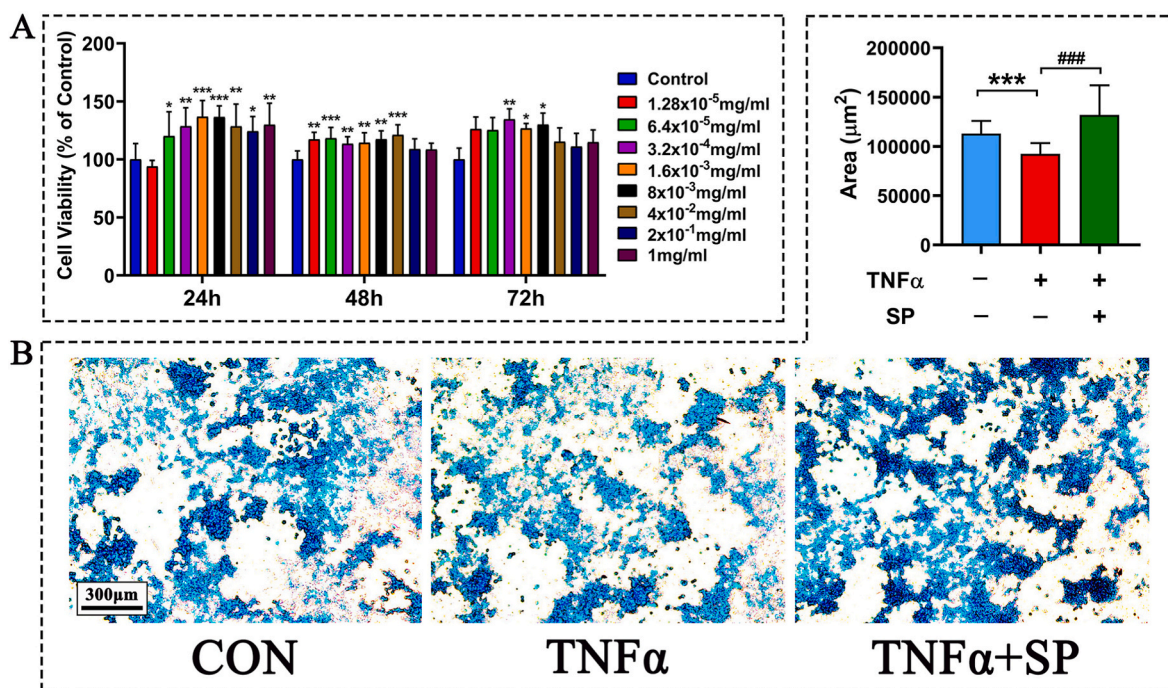

Figure 2. Effect of SP on cell viability and acidic glycoprotein secretion of C28 chondrocytes. (A)Cell viability of C28 chondrocytes incubated with various concentrations of SP for 24, 48 and 72 h. (B) Effect of 3.2×10^{-4} mg/ml SP on acidic glycoprotein secretion in C28 chondrocytes induced by 1 ng/ml TNFα for 10 days. Note: $^*P < 0.05$, $^{**}P < 0.01$, $^{***}P < 0.001$ *vs* Control; $^{\#}P < 0.05$, $^{\#\#}P < 0.01$, $^{\#\#\#}P < 0.001$ *vs* TNFα. Values are presented as mean ± SD.
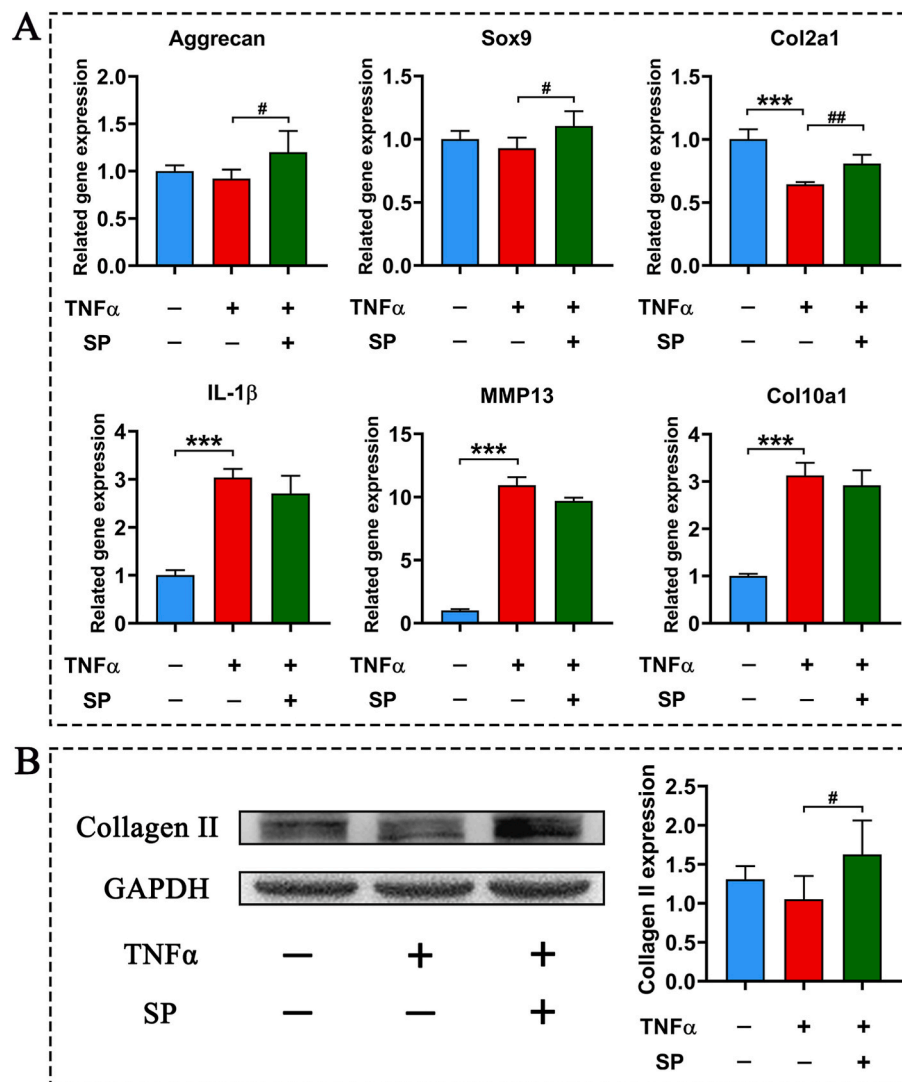
Figure 3. Effect of 3.2×10^{-4} mg/ml SP on the expression of chondrogenic products in C28 chondrocytes induced by 1 ng/ml TNFα. (A) *Aggrecan, Sox9, Col2a1, IL-1β, MMP13* and *Col10a1* gene expression in C28 chondrocytes induced by 1 ng/ml TNFα for 1 day determined by RT-qPCR. (B) Western blots show effects of 3.2×10^{-4} mg/ml SP on protein levels of Collagen II in C28 chondrocytes induced by 1 ng/ml TNFα for 10 days. Note: *$P < 0.05$, **$P < 0.01$, ***$P < 0.001$ *vs* Control; #$P < 0.05$, ##$P < 0.01$, ###$P < 0.001$ *vs* TNFα. Values are presented as mean ± SD.

in OA rats exhibited improvements in both bone and cartilage damage after SP treatment (Fig. 4). SP also alleviated the narrowing of the knee joint space in OA rats and reduced the histopathological score of the OA lesion area ($P < 0.01$) (Fig. 4). μ-CT scans of OA rats treated with SP showed significant relief in the bone damage to the medial femoral condyle and the subchondral bone surface of the tibial plateau (Fig. 5), with an increase in the BV/TV ratio, as well as the number and thickness of trabeculae in the area C of the injury, and a decrease in the thickness of the subchondral bone plate (Fig. 5). Moreover, SP treatment resulted in a 70.33 % decrease in the cartilage degeneration score ($P < 0.001$) and augmented the cartilage thickness and area by 80.49 % ($P < 0.01$) and 108.58 % ($P < 0.01$) respectively, when compared with OA rats (Fig. 6). Further, immunohistochemistry and immunofluorescence analyses revealed that the expression levels of Collagen II in the knee cartilage of the TNFα + SP group rose by 268.68 % ($P < 0.001$) and 342.46 % ($P < 0.001$) compared to OA rats, respectively (Fig. 6).

3.3. SP mitigated cartilage injury in C28 inflammatory chondrocytes through ITGβ1-PI3K-AKT signal axis

RNA sequencing analysis revealed that both TNFα induction and

subsequent SP treatment led to significant changes in gene expression within C28 chondrocytes (Fig. 7A). Compared to the normal control group, TNFα induction led to 5186 differentially expressed genes (DEGs) in C28 chondrocytes, comprising 2616 upregulated and 2570 downregulated genes (Fig. 7B). Furthermore, SP treatment to TNFα-induced C28 chondrocytes resulted in 2975 DEGs, including 1332 upregulated and 1643 downregulated genes compared to the TNFα group (Fig. 7B). Intersecting the DEGs from the TNFα/Control and SP/TNFα comparisons yielded a Venn diagram highlighting key potential targets for SP in the treatment of the chondrocyte inflammatory injury model (Fig. 7C). By analyzing the potential targets in Venn diagram, we identified the top 60 KEGG pathways and the top 60 GO enrichment items. KEGG enrichment analysis showed that the treatment of SP made ECM-receptor interaction ($Q = 0.12$), Focal adhesion ($Q = 0.02$) and PI3K-Akt signaling pathway ($Q = 0.03$) more active ($Q < 0.001$) in C28 inflammatory chondrocytes (Fig. 7D). Moreover, several GO enrichment items related to chondrogenesis, including inflammatory response (IR), apoptotic process (AP), extracellular matrix organization (EMO), cell adhesion (CA), collagen binding (CB), integrin binding (IB) and collagen-containing extracellular matrix (EMCC), exhibited significant changes following SP treatment ($Q < 0.001$) (Fig. 7E ~ G). Supplementary Figure S3~S9
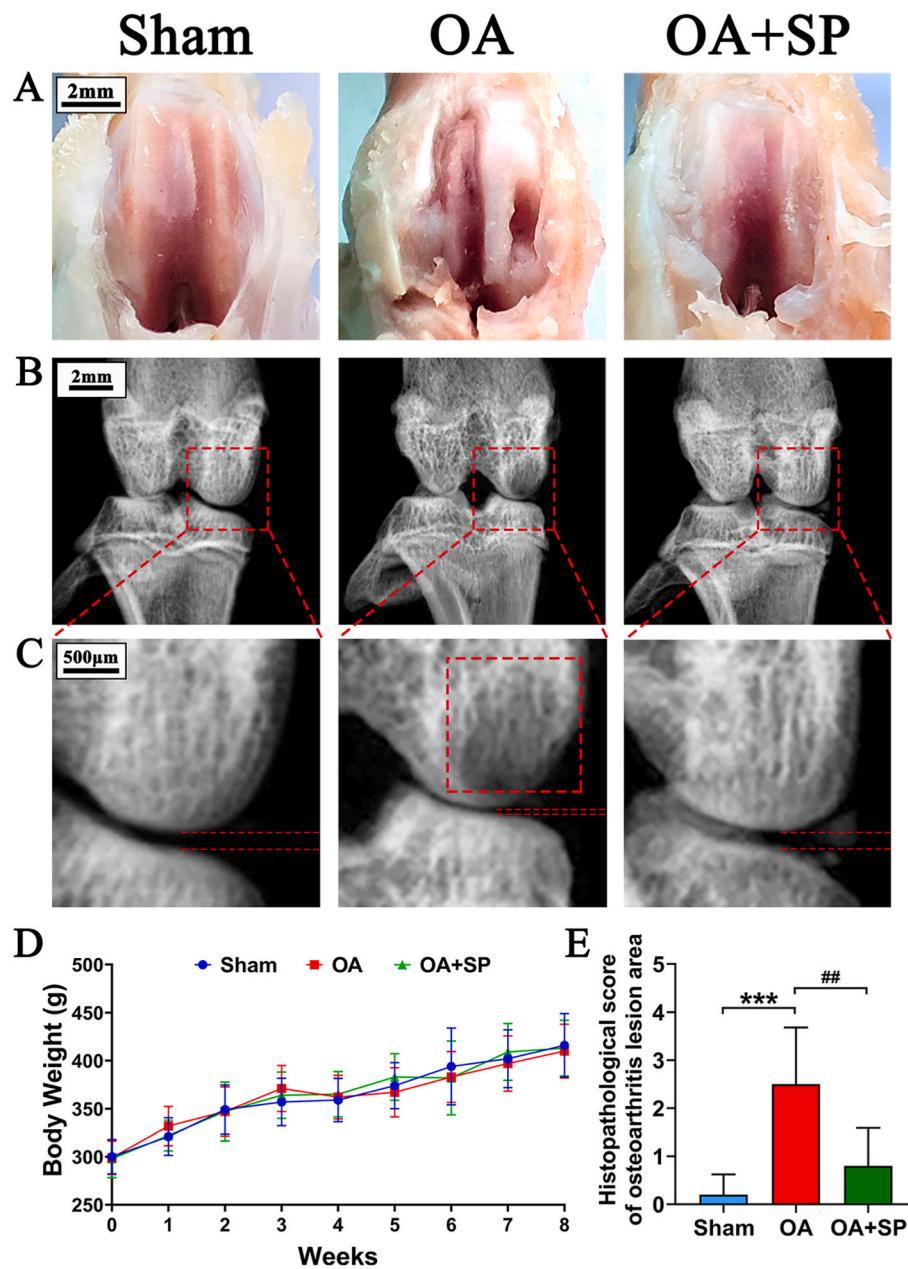
Figure 4. Effect of 200 mg/kg/day SP on weight and knee joint lesion in OA rats. (A) Representative images of knee joint in OA rats treated with 200 mg/kg/day SP. (B–C) Representative X-ray images of knee joint in OA rats treated with 200 mg/kg/day SP. (D) Body weight of OA rats treated with 200 mg/kg/day SP. (E) Histopathological score of osteoarthritis lesion area of OA rats treated with 200 mg/kg/day SP. N = 10 per group. Note: $*P < 0.05$, $**P < 0.01$, $***P < 0.001$ *vs* Sham; $^{\#}P < 0.05$, $^{\#\#}P < 0.01$, $^{\#\#\#}P < 0.001$ *vs* OA. Values are presented as mean ± SD.

demonstrate the bubble charts of KEGG and GO enrichment analysis. By analyzing the potential targets through KEGG pathway and GO enrichment items, the ITGB1-PI3K-AKT signaling axis was found to be a critical regulator in ameliorating the inflammatory injury in C28 inflammatory chondrocytes as a result of SP treatment. RT-qPCR results showed that SP enhanced gene expression of *ITGβ1*, *p110δ*, *AKT1*, *Col2a1* and *ACAN*. In contrast, TNFα intervention alone suppressed *ITGβ1* and *Col2a1* gene expression while upregulating *p110δ* and *AKT1* gene expression. The intervention of SP on TNFα-induced C28 chondrocytes enhanced the gene expression of *ITGβ1*, *p110δ*, *AKT1* and *Col2a1* (Fig. 8A). Conversely, ITGβ1 siRNA knock-down intervention downregulated *ITGβ1*, *p110δ*, *AKT1* and *ACAN* gene expression in C28 chondrocytes, which could not be completely reversed by intervention with SP (Fig. 8D). Western blot analyses complemented these findings, indicating that SP intervention enhanced the protein expression levels of

ITGβ1, p110δ, p-AKT1, and ACAN in C28 chondrocytes. TNFα intervention alone reduced ITGβ1 and ACAN protein levels but elevated protein levels of p110δ and p-AKT1. When SP was applied to TNFα-induced C28 chondrocytes, there was an stimulation in the protein expression of ITGβ1, p110δ, p-AKT1, and ACAN (Fig. 8B ~ C). Similar to the gene expression patterns, ITGβ1 siRNA knock-down intervention suppressed the protein levels of ITGβ1 and ACAN in C28 chondrocytes, which was not fully reversible by SP treatment (Fig. 8E ~ F). The results from the GO biological process analysis indicate that the significance of apoptosis process, which was initially ranked as NO.1, dropped to NO.6 following the intervention of SP in inflammatory C28 cells (Supplementary Figure S10D~E). Furthermore, the 2632 genes identified in the Venn diagram were utilized as the target gene set for gene set enrichment analysis (GSEA). The GSEA analysis revealed that the intervention with TNFα activated the apoptosis signaling pathway, whereas the
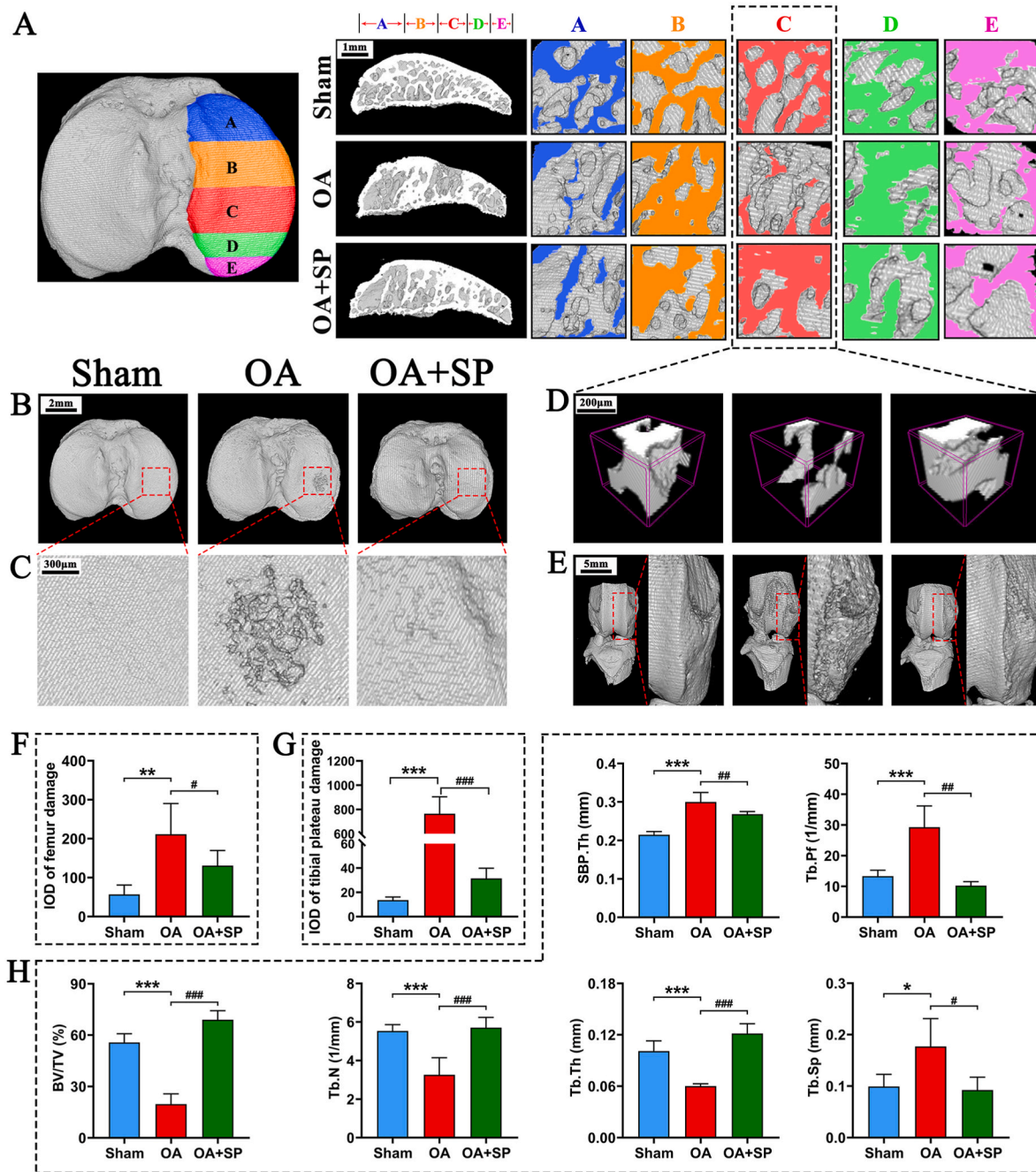
Figure 5. Representative images of μ-CT of knee joint in OA rats treated with 200 mg/kg/day SP. (A) Representative images of sclerosis and injury of subchondral bone of medial tibial plateau in OA rats treated with 200 mg/kg/day SP. (B–C) Representative images of medial tibial plateau surface injury in OA rats treated with 200 mg/kg/day SP. (D) Representative images of partial C region injury of subchondral bone of medial tibial plateau in OA rats treated with 200 mg/kg/day SP. (E) Representative images of medial femoral condyle injury of knee joint in OA rats treated with 200 mg/kg/day SP. Analysis of SP on (F) medial femoral condyle injury and (G) medial tibial plateau surface injury in OA rats. (H) Analysis of μ-CT images in (D). N = 6 per group. Note: $*P < 0.05$, $**P < 0.01$, $***P < 0.001$ *vs* Sham; $^{\#}P < 0.05$, $^{\#\#}P < 0.01$, $^{\#\#\#}P < 0.001$ *vs* OA. Values are presented as mean ± SD.

intervention with SP suppressed the expression of this pathway (Supplementary Figure S11A~B). By intersecting the top 20 differentially expressed genes (DEGs) from the TNFα/Control and TNFα+SP/TNFα comparisons within the apoptosis signaling pathway, a Venn diagram was generated, highlighting key potential targets for SP to alleviate chondrocyte apoptosis, including but not limited to ERN1, FAS, BID and ATF4 (Supplementary Fig. S11C).

4. Discussion

The results of this study reveal that SP markedly increased cell viability under normal conditions and enhanced the secretion of acidic glycoproteins in inflammatory induced C28 chondrocytes model, and elevated the expression of genes associated with chondrogenesis (*Aggrecan*, *Sox9*, *Col2a1*) as well as Collagen II protein in inflammatory environment. *In vivo*, SP treatment of OA rats significantly ameliorated knee joint stenosis and mitigated the damage to bone and cartilage tissue. Furthermore, SP treatment substantially increased the thickness
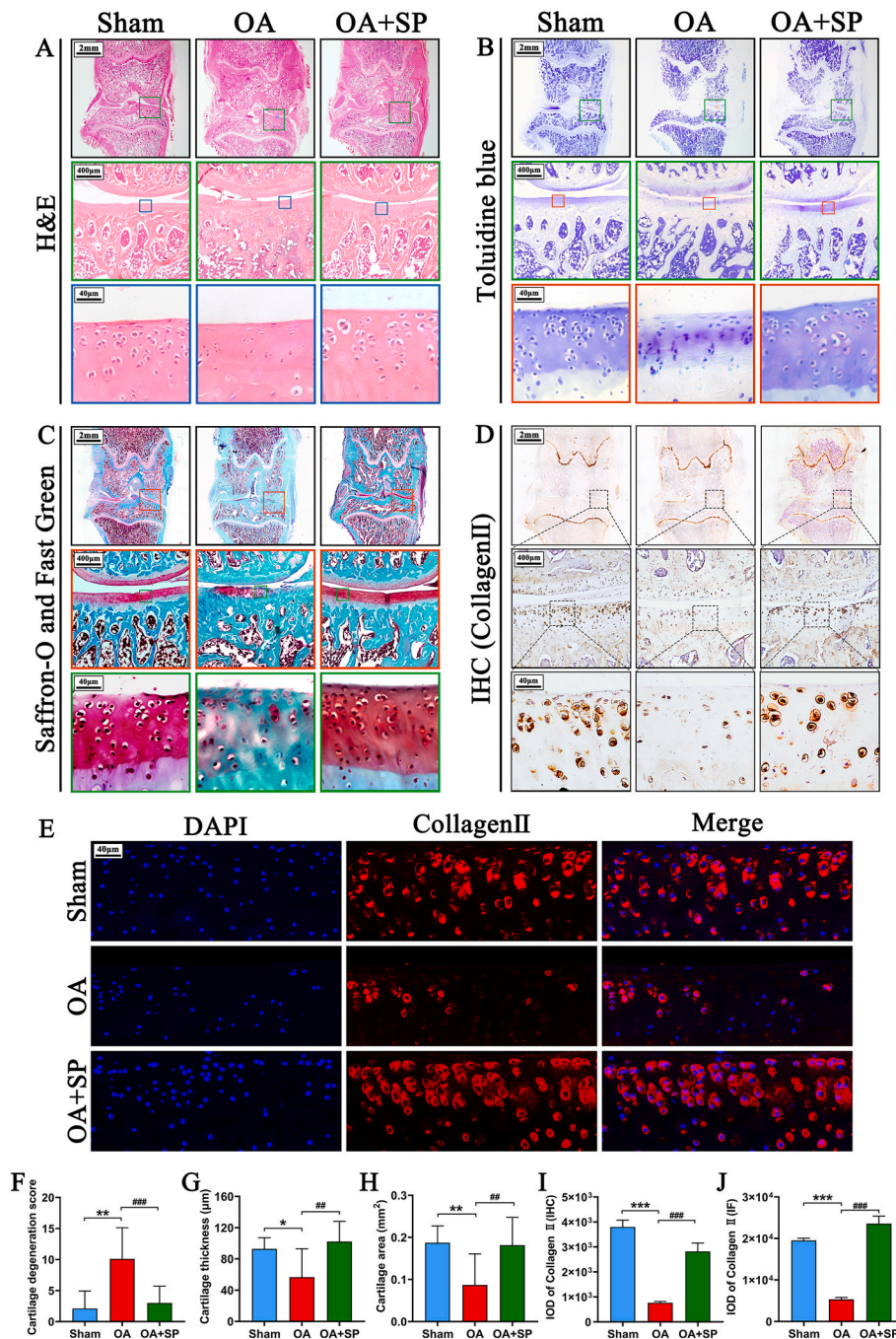
Figure 6. Representative images of (A) H&E staining (B) Toluidine blue staining (C) Saffron-O and Fast Green staining of knee joint in OA rats treated with 200 mg/kg/day SP. Representative images of (D) immunohistochemical staining and (E) immunofluorescence staining for Collagen II of knee joint in OA rats treated with 200 mg/kg/day SP. Effects of SP on (F) Cartilage degeneration score (G) Cartilage thickness (H) Cartilage area of knee joint in OA rats, N = 9 per group. Collagen II expression (I–J) of knee joint in OA rats treated with 200 mg/kg/day SP determined by immunohistochemical staining and immunofluorescence staining respectively, N = 3 per group. Note: *$P < 0.05$, **$P < 0.01$, ***$P < 0.001$ *vs* Sham; #$P < 0.05$, ##$P < 0.01$, ###$P < 0.001$ *vs* OA. Values are presented as mean ± SD. (For interpretation of the references to color in this figure legend, the reader is referred to the Web version of this article.)

and surface area of the cartilage on the tibial plateau, and notably boosted the expression of Collagen II in comparison to OA model. These promising outcomes position SP as a noteworthy candidate for OA treatment.

Existing research highlights that polysaccharide extracted from Sargassum possesses a range of therapeutic properties, including anti-inflammatory [29], anti-tumor [30], anti-oxidation [41], hypoglycemic [32,42] and hypolipidemic [33] effects. Moreover, previous studies have suggested that extracts from Sargassum can mitigate oxidative

stress and the inflammatory response in chondrocytes [43] as well as inhibit chondrocyte apoptosis [44]. In this study, we present findings regarding a purified Sargassum polysaccharide, which exhibits promising potential for the treatment of OA.

Prior research indicates that plant polysaccharides exhibit multi-target and multi-pathway characteristics [45]. Given the close association of polysaccharides with the energy metabolism of organisms [46, 47], we developed a chronic inflammatory injury cell model using C28 chondrocytes TNFα induction, subsequently intervening with SP for a
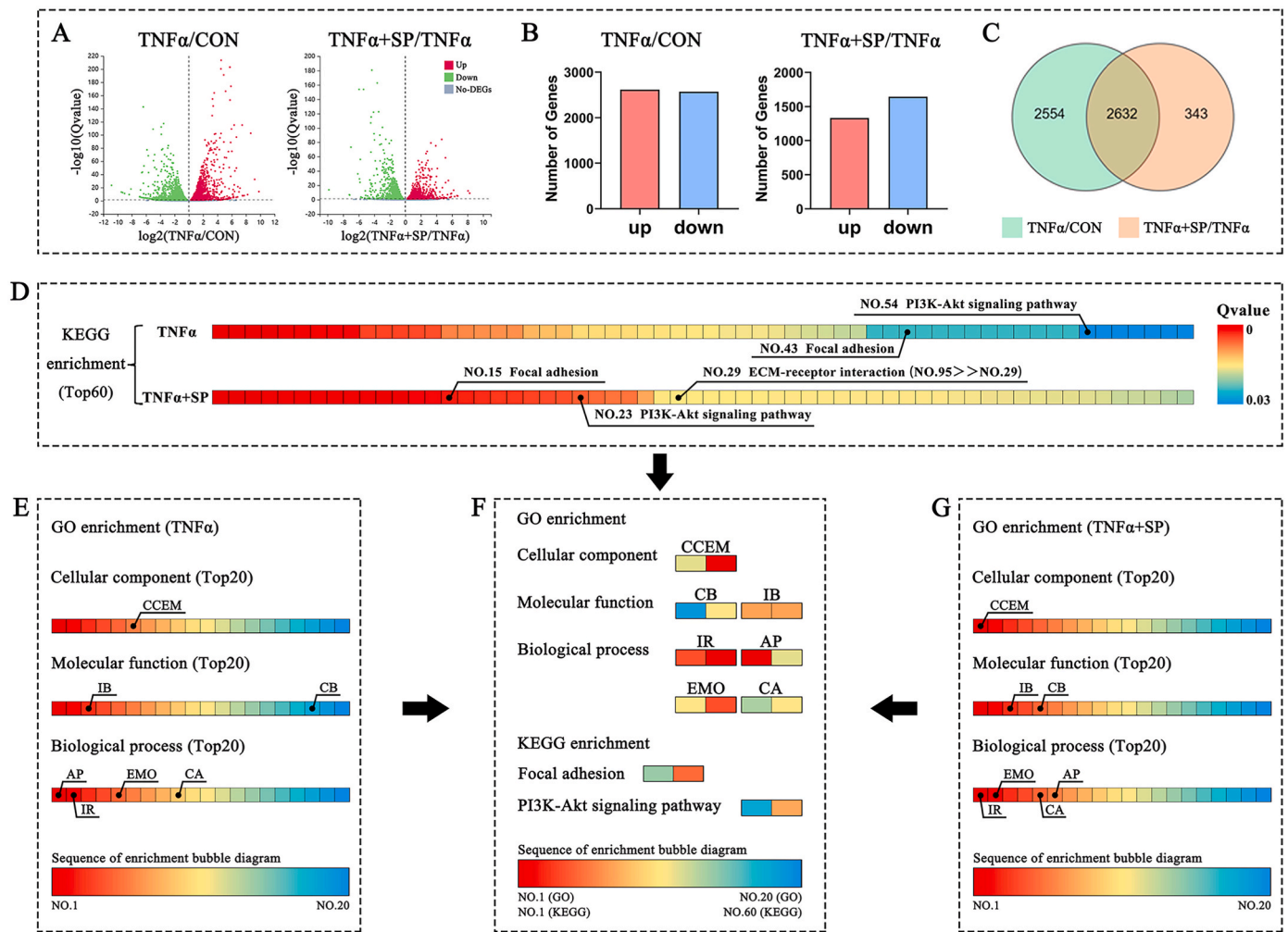
Figure 7. Analysis of RNA-seq. (A) Volcano map of differentially expressed genes (DEGs) in TNFα group (*vs* CON) and TNFα + SP group (*vs* TNFα). (B) Number of DEGs. (C) Venn diagram of DEGs. (D) Top 60 signal pathways in KEGG enrichment analysis. (E) Top 20 items of GO enrichment analysis in TNFα group (*vs* CON). (F) Potential targets obtained by KEGG enrichment and GO enrichment; the rectangle was divided into two equal parts (the left of rectangle represented GO items or KEGG pathway in TNFα group (*vs* CON) and the right of rectangle represented GO items or KEGG pathway in TNFα + SP group (*vs* TNFα). (G) Top 20 items of GO enrichment analysis in TNFα + SP group (*vs* TNFα). The colors in the rectangle represent the expression/ranking of KEGG pathway or GO items (red indicated up-regulation, blue indicated down-regulation). *CCEM*: collagen-containing extracellular matrix; *IB*: integrin binding; *CB*: collagen binding; *AP*: apoptotic process; *IR*: inflammatory response; *EMO*: extracellular matrix organization; *CA*: cell adhesion. (For interpretation of the references to color in this figure legend, the reader is referred to the Web version of this article.)

duration of 10 days. To explore the potential mechanisms, we investigated cellular biological processes through RNA-seq analysis. Initially, we identified GO enrichment items with substantial shifts in expression from the GO enrichment analysis. The GO enrichment analysis presented a significant uptick in activity for the "extracellular matrix organization" and "collagen-containing extracellular matrix" GO enrichment items after treating with SP, suggesting that SP enhances collagen production in the extracellular matrix of C28 inflammatory chondrocytes. Furthermore, the "cell adhesion" GO enrichment items also exhibited a notable increase in activity post-SP treatment, while "integrin binding" GO enrichment items consistently showed high activity levels. Subsequently, we identified the signaling pathways with manifested significant changes through KEGG enrichment analysis. In comparison with the TNFα-treated group, KEGG enrichment analysis revealed a significant upregulation of ECM-receptor interaction, focal adhesion and PI3K/AKT signal pathway following SP treatment. Based on the phenotypic outcomes, we combined both GO and KEGG enrichments analysis, revealing integrin signaling cascades involved both in ECM-receptor interaction and focal adhesion biological process, suggesting that the chondrogenesis effect of SP may close relate to the regulation of integrin signaling cascades.

Integrins, composed of α and β subunits, are heterodimeric transmembrane proteins that mediate cell-extracellular matrix (ECM) interactions and regulate various critical cellular functions such as proliferation, differentiation, survival, migration, tissue morphogenesis, and remodeling [48,49]. The human genome encodes at least eighteen α and eight β subunits; the β subunits primarily bind to cytoskeletal and cell signaling molecules, while the α subunits play a modulatory role [50]. Specifically, in the integrin β subfamily, ITGβ1 facilitates interactions between chondrocytes and matrix proteins, influencing essential chondrocyte processes including mechanical transduction, phenotype maintenance, gene expression regulation, and apoptosis prevention [50]. ITGβ1 is abundantly expressed in chondrocytes. Knock-down ITGβ1 expression exhibit altered chondrocyte morphology and varying degrees of chondrodysplasia due to diminished adherence to collagen type II, weakened fibronectin binding and spreading, and disorganized F-actin [51]. Prior research [52] has demonstrated that blocking antibodies specific for ITGβ1 promote cell apoptosis within a cartilage developmental model. Furthermore, this intervention impedes sternum growth. Conversely, ITGβ1 upregulation enhances aggrecan
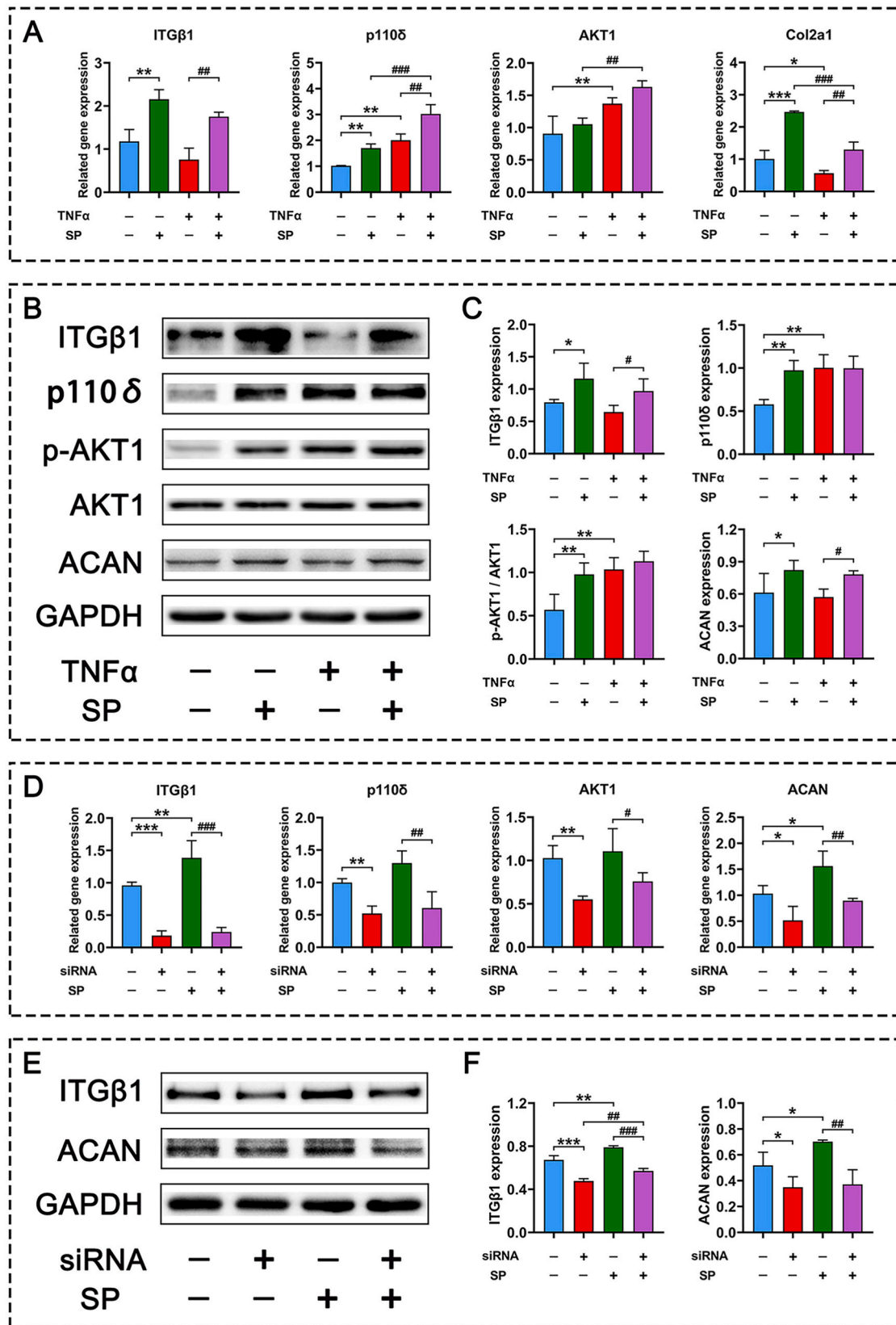
Figure 8. Regulation of 3.2×10^{-4} mg/ml SP on ITGβ1-PI3K-AKT signal axis in C28 chondrocytes. (A) *ITGβ1, p110δ, AKT1* and *Col2a1* gene expression in C28 chondrocytes induced by 1 ng/ml TNFα determined by RT-qPCR. (B) Western blots show effects of 3.2×10^{-4} mg/ml SP on protein levels of ITGβ1, p110δ, p-AKT1, AKT1 and ACAN in C28 chondrocytes induced by 1 ng/ml TNFα. (C) Protein levels of ITGβ1, p110δ, p-AKT1/AKT1 and ACAN. (D) *ITGβ1, p110δ, AKT1* and *ACAN* gene expression in C28 chondrocytes induced by ITGβ1 siRNA determined by RT-qPCR. (E) Western blots show effects of 3.2×10^{-4} mg/ml SP on protein expression of ITGβ1 and ACAN in C28 chondrocytes induced by ITGβ1 siRNA. (F) Protein levels of ITGβ1 and ACAN. Note: *$P < 0.05$, **$P < 0.01$, ***$P < 0.001$ *vs* Control or Negative control; #$P < 0.05$, ##$P < 0.01$, ###$P < 0.001$ *vs* TNFα + SP/ITGβ1 siRNA + SP. Values are presented as mean ± SD.

and type II collagen expression, encourages chondrocyte proliferation, and inhibits apoptosis [53]. In addition, ITGβ1 upregulation also stimulates cartilage matrix synthesis and enhances the mechanical integrity of the extracellular matrix (ECM) [54,55]. Acting as an intermediary between chondrocytes and the ECM, as a principal activator of FAK, ITGβ1 down-regulation compromises chondrocyte-ECM adhesion, impacting chondrocyte morphology and leading to an abnormal collagen fiber network [51]. Hence, our initial step was to confirm whether SP could enhance the expression of ITGβ1 in inflammatory C28 chondrocytes. Our results demonstrated that SP treatment up-regulated ITGβ1 gene and protein expression in chondrocyte impaired cell model.

In the downstream of the ITGβ1-regulated signaling cascade, FAK serves as a pivotal junction in the signal transduction network, where it primarily receives biological signals from integrins at its upstream and connects to downstream signaling cascades such as Wnt/β-catenin [56], ERK1/2 [57,58], PI3K/Akt [59,60] signaling pathways. FAK acts as an intermediary conduit between integrins and PI3K/AKT, transmitting extracellular signals received by integrins to the cell interior and triggering the PI3K/AKT pathway [61]. Recent research has indicated that activation of the PI3K/AKT signaling pathway can foster anabolic processes in the cartilage ECM, promote inflammation, stimulate chondrocyte proliferation, intensify subchondral bone sclerosis, and curtail chondrocyte apoptosis within the OA microenvironment [62]. Based on these insights, it is speculated that SP may modulates the PI3K/AKT signaling pathway via ITGβ1, thereby mitigating inflammatory injury in C28 inflammatory chondrocytes.

Thereafter, our performed related molecular biology experiment to verify our hypothesis. The results confirmed that SP treatment up-regulated ITGβ1, p110δ, p-AKT1, ACAN, and Col2a1 expressions to counteract the downregulation induced by TNFα on ITGβ1, ACAN, and Col2a1 expression in the TNFα-induced inflammatory C28 model. SP treatment significantly mitigated the repression of ITGβ1, ACAN, and Col2a1 expressions, and notably enhanced the expression of p110δ and p-AKT1. To further verified whether ITGβ1 is the main target of SP, ITGβ1 expression were knockdown by siRNA in C28 chondrocytes. The results demonstrated that knockdown of ITGβ1 decreased the expression of p110δ, AKT1, and ACAN, and this suppression was not entirely reversed by SP treatment, indicating that ITGβ1 is a critical target of SP. TNFα reduced ITGβ1 expression, but directly or indirectly still stimulated the PI3K-AKT pathway, contributing to inflammatory injury in C28 chondrocytes. SP activated the ITGβ1-PI3K-AKT signaling axis, thereby enhancing ECM-receptor interactions and cell adhesion, which establishes a conducive environment for the synthesis of collagen and proteoglycan.

In conclusion, our results suggest that SP's promotion of chondrogenesis is intimately linked to the activation of the ITGβ1-PI3K-AKT signaling axis (Fig. 9).

While the ITGβ1-PI3K-AKT signaling axis has been recognized for its role in regulating proliferation [63–66], migration [65,67] and metastasis [66,68] in cancer cells, its function extends beyond these processes. It has been implicated in inhibiting apoptosis in myofibroblasts [69] and neurons [70] as well. A previous study reported low-intensity pulsed ultrasound treatment also upregulated this signaling pathway in chondrocytes [60]. Recent studies have revealed that JD-312, a novel non-toxic small molecule, significantly enhances cartilage regeneration and boosts the expression of Col2a1 and Acan in a DMM rat model. The beneficial effects of JD-312 are at least in part mediated via upregulation of genes associated with the focal adhesion, PI3K-Akt signaling and the ECM-receptor interaction pathways [71]. However, there is no studies reported the use of polysaccharides to ameliorate cartilage degeneration through the modulation of the ITGβ1-PI3K-AKT signaling axis yet.

Our transcriptome analysis showed that ECM receptor and apoptosis signaling are the most relevant signaling cascades in the effects of SP. We first focus on the ECM receptor signaling cascades as it is more affected by SP treatment. In addition, our *in vitro* study demonstrated SP significantly stimulated cartilage ECM secretion. Therefore, we first pay more attention in this signaling cascade. However, preventing chondrocyte apoptosis may also be the potential mechanism in the effects of SP, as evidenced in Supplementary Figs. S10 and S11.

The GO biological process and GSEA analyses revealed that SP effectively inhibited the apoptosis process triggered by TNFα in C28 inflammatory cells. Among the potential targets identified, we consider ERN1, ATF4, BID and FAS worthy of further attention. Regarding ERN1, research indicates that ERN1 mRNA is the actual target of hcmv-miR-UL148D and its encoded protein IRE1α is translationally repressed by the overexpression of hcmv-miR-UL148D resulting in the attenuation of apoptosis [72]. Regarding ATF4, research has demonstrated that activated transcription factor 4 (ATF4) plays a pivotal role as the key transcription factor in ERS [73], and is at least partially implicated in ERS-mediated apoptosis [74]. Although the studies [73,74] focus on vascular calcification rather than osteoarthritis, they underscore the critical role of ATF4 in modulating endoplasmic reticulum stress and apoptosis. Concerning Bid, the study indicates that the concurrent elevation of Bim, Bid and Bad, along with reduced levels of Bcl-2 and Bcl-xl may render cells more susceptible to apoptosis during sepsis. Bim and Bid may become relevant therapeutic targets aim at inhibiting accelerated apoptosis in patients with severe sepsis [75]. FAS and its ligand, FasL, are recognized as markers of apoptosis [76].
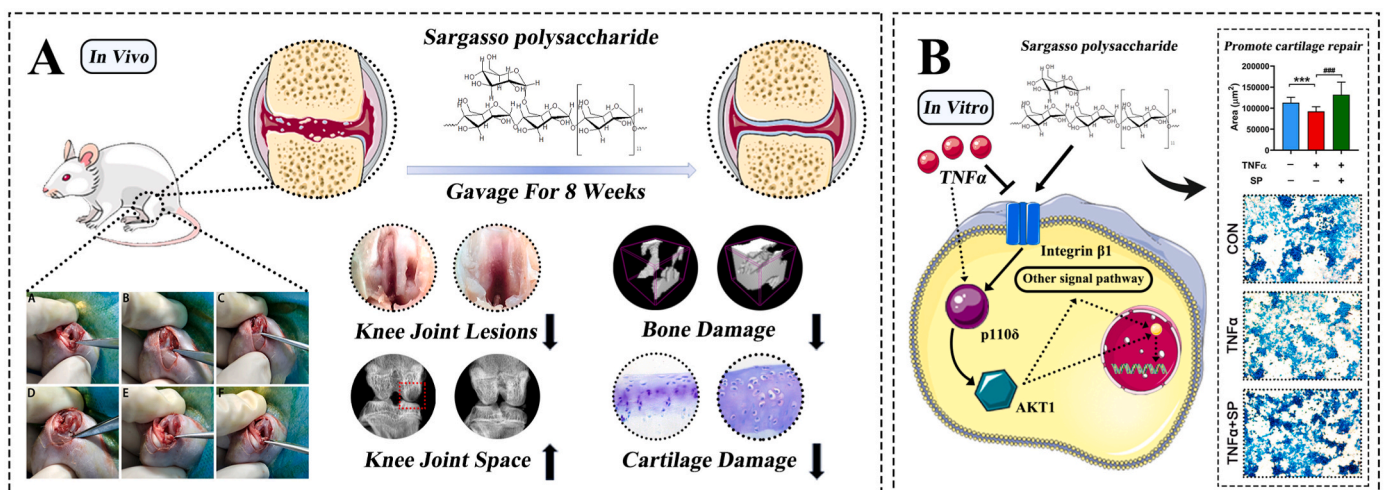

Figure 9. Graphic abstract of sargassum polysaccharide attenuates osteoarthritis in rats and is associated with the up-regulation of the ITGβ1-PI3K-AKT signaling pathway.

In the RNA-seq results, GSEA analysis revealed that the intervention of SP down-regulated the apoptosis signaling pathway activated by TNFα. This intervention also decreased the gene expression levels of *ERN1*, *ATF4*, *BID* and *FAS*. Consequently, we postulate that the potential mechanism of SP involves the prevention of chondrocyte apoptosis, as illustrated in Supplementary Figs. S10 and S11.

Glucosamine, as a successful polysaccharide-based drug, has been utilized in the treatment of OA since the 1960s, gaining widespread adoption in North America and globally by the late 20th century. Nonetheless, its efficacy in treating OA still cannot meet requirement of OA [77]. Our preliminary experimental results (Supplementary Fig. S2) also show that the therapeutic effect of glucosamine hydrochloride on OA is limited. Given glucosamine's limitations, the search for novel polysaccharides with consistent chondrogenic activity and stable therapeutic effects is highly significant. In our study, SP can protect inflammatory chondrocytes, enhance chondrogenesis *in vitro*, and slow down the progression of OA *in vivo*. The potential therapeutic targets and signaling pathways influenced by SP were also explored and identified. Our research marks the first instance unveiling the advantageous effects and underlying mechanisms of SP in OA treatment. With its clinical prospects, SP presents compelling new evidence for the advancement of a next-generation polysaccharide drug for OA therapy.

Limitations in our study: Firstly, the absence of a positive control group is notable in this study. However, in our preliminary investigation, we compared the efficacy of glucosamine hydrochloride (GH) and SP in treating OA rats (refer to Supplementary Fig. S2). GH, a commonly prescribed OA drug, was utilized as a positive control in our preliminary study, administered at doses consistent with clinical standards. The results indicated that the effects of SP in treating OA were superior to those of GH. Secondly, there is a lack of a comprehensive investigation to optimize the dosage of SP; we only selected a dose similar to the clinical standards for GH treatment. Thirdly, although we demonstrated that SP could activate the ITGβ1-PI3K-AKT signaling axis to facilitate cartilage repair, our study did not progress to the use of knockout (KO) mice to further validate these targets *in vivo*.

In conclusion, SP has demonstrated the ability to mitigate the inflammatory injury induced by TNFα and has been shown to ameliorate bone and cartilage injury in OA rats. Its influence on chondrogenesis is linked to the activation of the ITGβ1-PI3K-AKT signaling pathway. These findings provide important information for the promising potential of SP to be developed as an OA drug.

Funding information

Authorship

All persons who meet authorship criteria are listed as authors, and all authors certify that they have participated sufficiently in the work to take public responsibility for the content, including participation in the concept, design, analysis, writing, or revision of the manuscript. Each author certifies that this material or part thereof has not been published in another journal, that it is not currently submitted elsewhere, and that it will not be submitted elsewhere until a final decision regarding publication of the manuscript in Journal of Orthopaedic Translation has been made.

Indicate the specific contributions made by each author (list the authors' initials followed by their surnames, e.g., Y.L. Cheung). The name of each author must appear at least once in each of the three categories below.

Section I

The authors whose names are listed immediately below certify that they have NO affiliations with or involvement in any organization or entity with any financial interest (such as honoraria; educational grants; participation in speakers' bureaus; membership, employment, consultancies, stock ownership, or other equity interest; and expert testimony or patent-licensing arrangements), or non-financial interest (such as personal or professional relationships, affiliations, knowledge or beliefs) in the subject matter or materials discussed in this manuscript.

Declaration of AI and AI-assisted technologies in the writing process

During the preparation of this work the authors used [Chat GPT] only in order to improve the language and readability of their paper. After using this tool, the authors reviewed and edited the content as needed and take full responsibility for the content of the publication.

Declaration of competing interest

A conflict of interest occurs when an individual's objectivity is potentially compromised by a desire for financial gain, prominence, professional advancement or a successful outcome. The Editors of the *Journal of Orthopaedic Translation* strive to ensure that what is published in the Journal is as balanced, objective and evidence-based as possible. Since it can be difficult to distinguish between an actual conflict of interest and a perceived conflict of interest, the Journal requires authors to disclose all and any potential conflicts of interest.

Acknowledgements

Appendix A. Supplementary data

Supplementary data to this article can be found online at https://doi.org/10.1016/j.jot.2024.06.015.

References

[1] Abramoff B, Caldera FE. Osteoarthritis: pathology, diagnosis, and treatment options. Med Clin 2020;104(2):293–311.

[2] Hunter DJ, Bierma-Zeinstra S. Osteoarthritis. Lancet (London, England) 2019;393 (10182):1745–59.

[3] Yue L, Berman J. What is osteoarthritis? JAMA 2022;327(13):1300.

[4] Andrianakos AA, Kontelis LK, Karamitsos DG, Aslanidis SI, Georgountzos AI, Kaziolas GO, et al. Prevalence of symptomatic knee, hand, and hip osteoarthritis in Greece. The ESORDIG study. J Rheumatol 2006;33(12):2507–13.

[5] Cui A, Li H, Wang D, Zhong J, Chen Y, Lu H. Global, regional prevalence, incidence and risk factors of knee osteoarthritis in population-based studies. EClinicalMedicine 2020;29-30:100587.

[6] Shane Anderson A, Loeser RF. Why is osteoarthritis an age-related disease?, Best practice & research. Clin Rheumatol 2010;24(1):15–26.

[7] Snochowska A, Szmigielska P, Brzeziańska-Lasota E, Tomaszewski W. Genetic and epigenetic interactions in the etiopathogenesis of osteoarthritis. Selected molecular factors in OA etiopathogenesis. Ortop Traumatol Rehabil 2017;19(3):227–37.

[8] Sellam J, Berenbaum F. Is osteoarthritis a metabolic disease? Joint Bone Spine 2013;80(6):568–73.

[9] Peshkova M, Lychagin A, Lipina M, Di Matteo B, Anzillotti G, Ronzoni F, et al. Gender-related aspects in osteoarthritis development and progression: a review. Int J Mol Sci 2022;23(5).

[10] Brown TD, Johnston RC, Saltzman CL, Marsh JL, Buckwalter JA. Posttraumatic osteoarthritis: a first estimate of incidence, prevalence, and burden of disease. J Orthop Trauma 2006;20(10):739–44.

[11] Bestwick-Stevenson T, Ifesemen OS, Pearson RG, Edwards KL. Association of sports participation with osteoarthritis: a systematic review and meta-analysis. Orthopaedic journal of sports medicine 2021;9(6):23259671211004554.

[12] Vaughn IA, Terry EL, Bartley EJ, Schaefer N, Fillingim RB. Racial-ethnic differences in osteoarthritis pain and disability: a meta-analysis. J Pain 2019;20(6):629–44.

[13] Allen KD, Golightly YM. State of the evidence. Curr Opin Rheumatol 2015;27(3):276–83.

[14] Murray CJ, Vos T, Lozano R, Naghavi M, Flaxman AD, Michaud C, et al. Disability-adjusted life years (DALYs) for 291 diseases and injuries in 21 regions, 1990-2010: a systematic analysis for the Global Burden of Disease Study 2010. Lancet (London, England) 2012;380(9859):2197–223.

[15] Lima AC, Ferreira H, Reis RL. Neves NM. Biodegradable polymers: an update on drug delivery in bone and cartilage diseases. Expet Opin Drug Deliv 2019;16(8):795–813.

[16] Bannuru RR, Osani MC, Vaysbrot EE, Arden NK, Bennell K, Bierma-Zeinstra SMA, et al. OARSI guidelines for the non-surgical management of knee, hip, and polyarticular osteoarthritis. Osteoarthritis Cartilage 2019;27(11):1578–89.

[17] Cooper C, Chapurlat R, Al-Daghri N, Herrero-Beaumont G, Bruyère O, Rannou F, et al. Safety of oral non-selective non-steroidal anti-inflammatory drugs in osteoarthritis: what does the literature say? Drugs Aging 2019;36(Suppl 1):15–24.

[18] Schjerning AM, McGettigan P, Gislason G. Cardiovascular effects and safety of (non-aspirin) NSAIDs. Nat Rev Cardiol 2020;17(9):574–84.

[19] Whelton A. Nephrotoxicity of nonsteroidal anti-inflammatory drugs: physiologic foundations and clinical implications. Am J Med 1999;106(5b):13s–24s.

[20] Cheng OT, Souzdalnitski D, Vrooman B, Cheng J. Evidence-based knee injections for the management of arthritis. Pain Med 2012;13(6):740–53.

[21] Bowman S, Awad ME, Hamrick MW, Hunter M, Fulzele S. Recent advances in hyaluronic acid based therapy for osteoarthritis. Clin Transl Med 2018;7(1):6.

[22] Deligiannidou GE, Papadopoulos RE, Kontogiorgis C, Detsi A, Bezirtzoglou E, Constantinides T. Unraveling natural products' role in osteoarthritis management-an overview. Antioxidants 2020;9(4):348.

[23] Pérez-Lozano ML, Cesaro A, Mazor M, Esteve E, Berteina-Raboin S, Best TM, et al. Emerging natural-product-based treatments for the management of osteoarthritis. Antioxidants 2021;10(2).

[24] Varela-Eirin M, Loureiro J, Fonseca E, Corrochano S, Caeiro JR, Collado M, et al. Cartilage regeneration and ageing: targeting cellular plasticity in osteoarthritis. Ageing Res Rev 2018;42:56–71.

[25] Baei P, Daemi H, Aramesh F, Baharvand H, Eslaminejad MB. Advances in mechanically robust and biomimetic polysaccharide-based constructs for cartilage tissue engineering. Carbohydr Polym 2023;308:120650.

[26] Roman-Blas JA, Castañeda S, Sánchez-Pernaute O, Largo R, Herrero-Beaumont G. Combined treatment with chondroitin sulfate and glucosamine sulfate shows No superiority over placebo for reduction of joint pain and functional impairment in patients with knee osteoarthritis: a six-month multicenter, randomized, double-blind, placebo-controlled clinical trial. Arthritis Rheumatol 2017;69(1):77–85.

[27] Wandel S, Jüni P, Tendal B, Nüesch E, Villiger PM, Welton NJ, et al. Effects of glucosamine, chondroitin, or placebo in patients with osteoarthritis of hip or knee: network meta-analysis. BMJ (Clinical research ed.) 2010;341:c4675.

[28] Catarino MD, Silva-Reis R, Chouh A, Silva S, Braga SS, Silva AMS, et al. Applications of antioxidant secondary metabolites of sargassum spp. Mar Drugs 2023;21(3):172.

[29] Chen HL, Tan HL, Yang J, Wei YY, Hu TJ. Sargassum polysaccharide inhibits inflammatory response in PCV2 infected-RAW264.7 cells by regulating histone acetylation. Carbohydr Polym 2018;200:633–40.

[30] Shao P, Chen X, Sun P. Chemical characterization, antioxidant and antitumor activity of sulfated polysaccharide from Sargassum horneri. Carbohydr Polym 2014;105:260–9.

[31] Kang MC, Lee H, Choi HD, Jeon YJ. Antioxidant properties of a sulfated polysaccharide isolated from an enzymatic digest of Sargassum thunbergii. Int J Biol Macromol 2019;132:142–9.

[32] Cao C, Li C, Chen Q, Huang Q, Pérez MEM, Fu X. Physicochemical characterization, potential antioxidant and hypoglycemic activity of polysaccharide from Sargassum pallidum. Int J Biol Macromol 2019;139:1009–17.

[33] Kolsi RBA, Salah HB, Jardak N, Chaaben R, Jribi I, Feki AE, et al. Sulphated polysaccharide isolated from Sargassum vulgare: characterization and hypolipidemic effects. Carbohydr Polym 2017;170:148–59.

[34] Wu K, Gong Z, Zou L, Ye H, Wang C, Liu Y, et al. Sargassum integerrimum inhibits oestrogen deficiency and hyperlipidaemia-induced bone loss by upregulating nuclear factor (erythroid-derived 2)-like 2 in female rats. Journal of orthopaedic translation 2019;19:106–17.

[35] Deng L, Feng Z, Zheng H, Li X, Wu X, Quan W, et al. Isolation and characterization of a novel homopolysaccharide (SFP-1) from Sargassum fusiforme: promising anti-osteoporosis activity by modulating adipo-osteogenic differentiation. Ind Crop Prod 2024;207:117749.

[36] Smits P, Bolton AD, Funari V, Hong M, Boyden ED, Lu L, et al. Lethal skeletal dysplasia in mice and humans lacking the golgin GMAP-210. N Engl J Med 2010;362(3):206–16.

[37] Debnath S, Yallowitz AR, McCormick J, Lalani S, Zhang T, Xu R, et al. Discovery of a periosteal stem cell mediating intramembranous bone formation. Nature 2018;562(7725):133–9.

[38] McCarty MF. Glucosamine for wound healing. Med Hypotheses 1996;47(4):273–5.

[39] Barclay TS, Tsourounis C, McCart GM. Glucosamine. Ann Pharmacother 1998;32(5):574–9.

[40] Wang CJ, Cheng JH, Chou WY, Hsu SL, Chen JH, Huang CY. Changes of articular cartilage and subchondral bone after extracorporeal shockwave therapy in osteoarthritis of the knee. Int J Med Sci 2017;14(3):213–23.

[41] Zhao Y, Chen J, Ding Y, Luo M, Tong Y, Hu T, et al. A novel polysaccharide from sargassum weizhouense: extraction optimization, structural characterization, antiviral and antioxidant effects. Antioxidants 2023;12(10):1832.

[42] Li ZR, Jia RB, Wu J, Lin L, Ou ZR, Liao B, et al. Sargassum fusiforme polysaccharide partly replaces acarbose against type 2 diabetes in rats. Int J Biol Macromol 2021;170:447–58.

[43] Park C, Jeong JW, Lee DS, Yim MJ, Lee JM, Han MH, et al. Sargassum serratifolium extract attenuates interleukin-1β-induced oxidative stress and inflammatory response in chondrocytes by suppressing the activation of NF-κB, p38 MAPK, and PI3K/akt. Int J Mol Sci 2018;19(8):2308.

[44] Park C, Hong SH, Shin SS, Lee DS, Han MH, Cha HJ, et al. Activation of the Nrf2/HO-1 signaling pathway contributes to the protective effects of sargassum serratifolium extract against oxidative stress-induced DNA damage and apoptosis in SW1353 human chondrocytes. Int J Environ Res Publ Health 2018;15(6):1173.

[45] Kuang S, Liu L, Hu Z, Luo M, Fu X, Lin C, et al. A review focusing on the benefits of plant-derived polysaccharides for osteoarthritis. Int J Biol Macromol 2023;228:582–93.

[46] Wang M, Xie Z, Li L, Chen Y, Li Y, Wang Y, et al. Supplementation with compound polysaccharides contributes to the development and metabolic activity of young rat intestinal microbiota. Food Funct 2019;10(5):2658–75.

[47] Wei H, Lin X, Liu L, Peng X. Flaxseed polysaccharide alters colonic gene expression of lipid metabolism and energy metabolism in obese rats. Foods 2022;11(13):1991.

[48] Bachmann M, Kukkurainen S, Hytönen VP, Wehrle-Haller B. Cell adhesion by integrins. Physiol Rev 2019;99(4):1655–99.

[49] Loeser RF. Integrins and chondrocyte-matrix interactions in articular cartilage, Matrix biology. journal of the International Society for Matrix Biology 2014;39:11–6.

[50] Shakibaei M, Csaki C, Mobasheri A. Diverse roles of integrin receptors in articular cartilage. Adv Anat Embryol Cell Biol 2008;197:1–60.

[51] Aszodi A, Hunziker EB, Brakebusch C, Fässler R. Beta1 integrins regulate chondrocyte rotation, G1 progression, and cytokinesis. Gene Dev 2003;17(19):2465–79.

[52] Hirsch MS, Lunsford LE, Trinkaus-Randall V, Svoboda KK. Chondrocyte survival and differentiation in situ are integrin mediated. Dev Dynam : an official publication of the American Association of Anatomists 1997;210(3):249–63.

[53] Zhang LQ, Zhao GZ, Xu XY, Fang J, Chen JM, Li JW, et al. Integrin-β1 regulates chondrocyte proliferation and apoptosis through the upregulation of GIT1 expression. Int J Mol Med 2015;35(4):1074–80.

[54] Liang W, Zhu C, Liu F, Cui W, Wang Q, Chen Z, et al. Integrin β1 gene therapy enhances in vitro creation of tissue-engineered cartilage under periodic mechanical stress. Cell Physiol Biochem : international journal of experimental cellular physiology, biochemistry, and pharmacology 2015;37(4):1301–14.

[55] Zhang W, Lu W, Yu Q, Liu X, Jiang H. Upregulated desmin/integrin β1/MAPK axis promotes elastic cartilage regeneration with increased ECM mechanical strength. Int J Biol Sci 2023;19(9):2740–55.

[56] Fan C, Wu Z, Cooper DML, Magnus A, Harrison K, Eames BF, et al. Activation of focal adhesion kinase restores simulated microgravity-induced inhibition of osteoblast differentiation via wnt/B-catenin pathway. Int J Mol Sci 2022;23(10):5593.

[57] Liang W, Ren K, Liu F, Cui W, Wang Q, Chen Z, et al. Periodic mechanical stress stimulates the FAK mitogenic signal in rat chondrocytes through ERK1/2 activity. Cell Physiol Biochem : international journal of experimental cellular physiology, biochemistry, and pharmacology 2013;32(4):915–30.

[58] Xia P, Shen S, Lin Q, Cheng K, Ren S, Gao M, et al. Low-intensity pulsed ultrasound treatment at an early osteoarthritis stage protects rabbit cartilage from damage via the integrin/focal adhesion kinase/mitogen-activated protein kinase signaling pathway. J Ultrasound Med : official journal of the American Institute of Ultrasound in Medicine 2015;34(11):1991–9.

[59] Hanks SK, Ryzhova L, Shin NY, Brábek J. Focal adhesion kinase signaling activities and their implications in the control of cell survival and motility. Front Biosci : a journal and virtual library 2003;8:d982–96.

[60] Cheng K, Xia P, Lin Q, Shen S, Gao M, Ren S, et al. Effects of low-intensity pulsed ultrasound on integrin-FAK-PI3K/Akt mechanochemical transduction in rabbit osteoarthritis chondrocytes. Ultrasound Med Biol 2014;40(7):1609–18.

[61] Huang Y, Liao J, Vlashi R, Chen G. Focal adhesion kinase (FAK): its structure, characteristics, and signaling in skeletal system. Cell Signal 2023;111:110852.

[62] Sun K, Luo J, Guo J, Yao X, Jing X, Guo F. The PI3K/AKT/mTOR signaling pathway in osteoarthritis: a narrative review. Osteoarthritis Cartilage 2020;28(4):400–9.

[63] Lyu S, Ding X, Ye H, Guo R, Wu M, Cao L. KLF14 targets ITGB1 to inhibit the progression of cervical cancer via the PI3K/AKT signalling pathway, Discover. Oncology 2022;13(1):30.

[64] Zhang Y, Wu Z, Yu H, Wang H, Liu G, Wang S, et al. Chinese herbal medicine wenxia changfu formula reverses cell adhesion-mediated drug resistance via the integrin β1-PI3K-AKT pathway in lung cancer. J Cancer 2019;10(2):293–304.

[65] Wu R, Gao Y, Wu J, Wang C, Yang L. Semi-synthetic product dihydroartemisinin inhibited fibronectin-1 and integrin-β1 and interfered with the migration of HCCLM6 cells via PI3K-AKT pathway. Biotechnol Lett 2020;42(6):917–26.

[66] Guo D, Zhang D, Ren M, Lu G, Zhang X, He S, et al. THBS4 promotes HCC progression by regulating ITGB1 via FAK/PI3K/AKT pathway. Faseb J 2020;34(8): 10668–81. official publication of the Federation of American Societies for Experimental Biology.

[67] Qin J, Tang J, Jiao L, Ji J, Chen WD, Feng GK, et al. A diterpenoid compound, excisanin A, inhibits the invasive behavior of breast cancer cells by modulating the integrin β1/FAK/PI3K/AKT/β-catenin signaling. Life Sci 2013;93(18–19):655–63.

[68] Casar B, Rimann I, Kato H, Shattil SJ, Quigley JP, Deryugina EI. In vivo cleaved CDCP1 promotes early tumor dissemination via complexing with activated β1 integrin and induction of FAK/PI3K/Akt motility signaling. Oncogene 2014;33(2): 255–68.

[69] Zhang Y, Li H, Lian Z, Li N. Myofibroblasts protect myoblasts from intrinsic apoptosis associated with differentiation via β1 integrin-PI3K/Akt pathway. Dev Growth Differ 2010;52(8):725–33.

[70] Yang L, Zhu J, Yang L, Gan Y, Hu D, Zhao J, et al. SCO-spondin-derived peptide NX210 rescues neurons from cerebral ischemia/reperfusion injury through modulating the Integrin-β1 mediated PI3K/Akt pathway. Int Immunopharm 2022; 111:109079.

[71] Gao J, Pei H, Lv F, Niu X, You Y, He L, et al. JD-312 - A novel small molecule that facilitates cartilage repair and alleviates osteoarthritis progression. Journal of orthopaedic translation 2024;44:60–71.

[72] Pandeya A, Khalko RK, Singh S, Kumar M, Gosipatala SB. Hcmv-miR-UL148D regulates the staurosporine-induced apoptosis by targeting the Endoplasmic Reticulum to Nucleus signaling 1(ERN1). PLoS One 2022;17(9):e0275072.

[73] Shi Y, Zheng Z, Luo J, Li Y, He S, Shen X, et al. Possible effects of fibroblast growth factor 21 on vascular calcification via suppressing activating transcription factor 4 mediated apoptosis and osteogenic transformation in rats. Cell Biochem Funct 2022;40(4):349–58.

[74] Duan XH, Chang JR, Zhang J, Zhang BH, Li YL, Teng X, et al. Activating transcription factor 4 is involved in endoplasmic reticulum stress-mediated apoptosis contributing to vascular calcification, Apoptosis. an international journal on programmed cell death 2013;18(9):1132–44.

[75] Weber SU, Schewe JC, Lehmann LE, Müller S, Book M, Klaschik S, et al. Induction of Bim and Bid gene expression during accelerated apoptosis in severe sepsis. Crit Care 2008;12(5):R128.

[76] Huttunen R, Syrjänen J, Vuento R, Laine J, Hurme M, Aittoniemi J. Apoptosis markers soluble Fas (sFas), Fas Ligand (FasL) and sFas/FasL ratio in patients with bacteremia: a prospective cohort study. J Infect 2012;64(3):276–81.

[77] Clegg DO, Reda DJ, Harris CL, Klein MA, O'Dell JR, Hooper MM, et al. Glucosamine, chondroitin sulfate, and the two in combination for painful knee osteoarthritis. N Engl J Med 2006;354(8):795–808.